

See discussions, stats, and author profiles for this publication at: <https://www.researchgate.net/publication/274509798>

Density Functional Theory Calculations for the Structural, Electronic, and Magnetic Properties of $(\text{Gd}_2\text{O}_3)_n$ Clusters with $n = 1-10$

ARTICLE in THE JOURNAL OF PHYSICAL CHEMISTRY C · MARCH 2015

Impact Factor: 4.77 · DOI: 10.1021/acs.jpcc.5b00887

READS

46

2 AUTHORS, INCLUDING:



Xiuli Xia

Sun Yat-Sen University

1 PUBLICATION 0 CITATIONS

SEE PROFILE

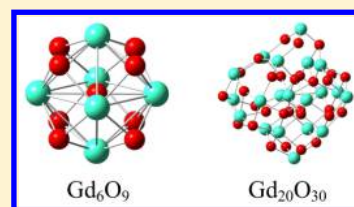
Density Functional Theory Calculations for the Structural, Electronic, and Magnetic Properties of $(\text{Gd}_2\text{O}_3)_n^{0,\pm 1}$ Clusters with $n = 1-10$

Xiuli Xia, Wenyong Hu, and Yuanzhi Shao*

State Key Laboratory of Optoelectronic Materials and Technologies, School of Physics and Engineering, Sun Yat-Sen University, Guangzhou 510275, People's Republic of China

Supporting Information

ABSTRACT: The structural stability and electronic and magnetic properties of stoichiometric $(\text{Gd}_2\text{O}_3)_n$ clusters with $n = 1-10$ were investigated using spin-polarized density functional theory through the broken-symmetry approach. Size-induced changes in the point symmetry of these clusters were observed. A large coordination number led to elongation of Gd–O bonding. Either adding an electron to or removing an electron from the ground state of a neutral cluster brought significant changes in the van der Waals volume for clusters $n = 1-3$. Binding energy increased with cluster size. However, the highest occupied molecular orbital–lowest unoccupied molecular orbital gap, ionization, and electron affinity fluctuated when n increased from 1 to 10. Natural population analysis and partial density of states revealed that the Gd-4f orbital hardly participated in bonding and that the Gd-5d/6s/6p orbitals were hybrid with the O-2p orbitals. The competition between Ruderman–Kittel–Kasuya–Yosida-type and superexchange-type interactions resulted in the magnetic oscillation of clusters between antiferromagnetic and ferromagnetic states. We also found similar behavior in the various structures of $\text{Gd}_{12}\text{O}_{18}$. The ground state was easily activated to the excited state because the antiferromagnetic and ferromagnetic coupling states were nearly identical in energy.



I. INTRODUCTION

Lanthanide elements and their compounds are important in many technological areas, such as electronics, magnetics, optics, biomedics, and catalyst converters.^{1–5} Among these materials, gadolinium oxide (Gd_2O_3) nanoparticles are of particular interest because of their peculiar magnetic behavior. Besides their use as contrast agents in medical magnetic resonance imaging, they have the potential to act as multimodal imaging and therapeutic agents.^{6–8} For example, the gadolinium-doped mesoporous silica nanocomposite $\text{Gd}_2\text{O}_3\text{--}@MCM\text{--}41$ holds the promising prospect of development as a targeted cell probe for cancer in vivo.⁹ Recently, Chen and co-workers studied the properties of Gd_2O_3 nanoparticles of various sizes and stoichiometries using density functional theory,¹⁰ but they calculated only the energy of antiferromagnetic (AFM) ground states in $(\text{Gd}_2\text{O}_3)_n$ with $n = 1-4$. The dependence of average bonding length on both the Gd–O coordination number and cluster size were not addressed in detail. Continuing this effort, we aim to understand the physical properties of stoichiometric $(\text{Gd}_2\text{O}_3)_n$ clusters with $n = 1-10$ through a different methodology.

Gd_2O_3 nanoparticles can exist in several morphologies, such as nanotubes,¹¹ nanoplates,¹² nanorods and microrods,¹³ and hollow spheres,¹⁴ demonstrating the advantage of forming new nanostructures. In addition, these particles are easy to dope with other lanthanide ions^{15,16} and have better chemical and thermal stability. The trivalent gadolinium ion Gd^{3+} owns seven unpaired electrons, which give rise to large atomic magnetic moments. Pedersen and Ojamäe¹⁷ and Ning et al.¹⁸ studied magnetic coupling in the $\text{Gd}_{12}\text{O}_{18}$ cluster by adopting the same

bulklike structure, but they arrived at opposite conclusions. Few studies have focused on $(\text{Gd}_2\text{O}_3)_n$ clusters, leaving the ground state of gadolinium nanoparticles in debate. A series of hollow and luminescent $\text{SiO}_2@\text{Gd}_2\text{O}_3\text{:Yb/Tm}$ capsules have been synthesized, which show great promise for use in drug delivery and cancer therapy.⁷ Therefore, understanding the intrinsic physical mechanism of the stoichiometric clusters is worthwhile for the sake of application.

We performed extensive density functional theory calculations for the structural, electronic, and magnetic properties of $(\text{Gd}_2\text{O}_3)_n^{0,\pm 1}$ clusters with $n = 1-10$. The average binding length, average coordination number, van der Waals volume, and point group symmetry of $(\text{Gd}_2\text{O}_3)_n$ clusters were collected as functions of Gd_2O_3 unit n . The problems of fundamental and highest occupied molecular orbital–lowest unoccupied molecular orbital (HOMO–LUMO) gap are also discussed. We addressed the exchange coupling and transition between the AFM and ferromagnetic (FM) states of $(\text{Gd}_2\text{O}_3)_n$ clusters and found that the magnetism of the ground-stated clusters fluctuated between AFM and FM with growing size. The paper is organized as follows. Section II deals with the computational details used in the work. The results and discussion are given in section III. Finally, a conclusion is presented in section IV.

Received: January 28, 2015

Revised: March 23, 2015

II. COMPUTATIONAL DETAILS

The calculations were performed on neutral and ionic Gd_2O_3 clusters, $(\text{Gd}_2\text{O}_3)_n^{0,\pm 1}$ with $n = 1-10$, using the Gaussian09 program.¹⁹ Initial guesses for stoichiometric nanoparticles were made from analogous metal sesquioxides, such as Gd_2O_3 ,¹⁰ Al_2O_3 ,^{14,20,21} Fe_2O_3 ,²² Ga_2O_3 ,¹³ In_2O_3 ,²³ Y_2O_3 ,²⁴ La_2O_3 ,²⁵ and B_2O_3 .²⁶ Following previous studies on Gd_2O_3 clusters,^{18,27-30} we performed the first-principles spin-polarized calculations with the broken-symmetry approach by using the B3LYP density functional.^{27,31} The Gview5 program was used to visualize these structures and determine their symmetry.¹⁹ We used the relativistic effective core potential (ECP) of the CEP-31G³²⁻³⁴ basis set for Gd atoms and the 6-31G(d)^{35,36} basis set for O atoms. The $5s^25p^64f^5d^16s^2$ shell (18 electrons) for Gd atoms and the $1s^22s^22p^4$ shell (8 electrons) for O atoms were taken into account explicitly in the spin-polarized density functional theory (SDFT) calculations.

As we treated α and β molecular orbitals separately in the open-shell spin system, the problem of inherent spin contamination would occur with the SDFT approach. We accepted a result rationally when its spin contamination after annihilation was less than 1% of the total. The convergence threshold was set as follows: 3×10^{-4} au/Å for the energy gradient, 1.2×10^{-3} Å for the atomic displacement, and 1×10^{-8} au for total energy. The optimized atomic structures were validated by checking the stability of wave functions as global minima. Furthermore, we used the Mutiwnf3.5 package to perform wave function analyses such as average bond length and average coordinate number, and plotted the total and partial density of states (TDOS and PDOS).³⁷ The benchmark calculations are shown in section 1 of Supporting Information.

III. RESULTS AND DISCUSSION

A. Geometrical Structures. A few typical low-lying isomers of $(\text{Gd}_2\text{O}_3)_n$ clusters with $n = 1-10$ and their relative energies are shown in Figure 1. The equilibrium geometries are labeled by their point group symmetry and relative energy with respect to the energy (taken to be zero) of the ground state. Obviously, cluster symmetry reduces with increasing cluster size n . Although quite different from analogous clusters X_2O_3 ($\text{X} = \text{Gd}$,¹⁰ Al ,^{14,20,21} Fe ,²² Ga ,¹³ In ,²³ Y ,²⁴ La ,²⁵ and B)²⁶, the size-induced effects on the symmetry of the clusters are in accordance with the size-induced changes in the crystal lattice symmetry.^{2,38}

The size-induced transformation in crystal symmetry may shed light on the distortion of Gd_2O_3 clusters. Surface tension and ionic character decrease with increasing physical dimensions of the particle, which gives rise to the reduction of symmetry for large particles.^{2,38} Ayyub et al. reported that the crystal lattice tends to transform into a structure of higher symmetry with decreasing crystal size.³⁸ For instance, hexagonal phase (anisotropic) NaYF_4 transforms into a cubic phase (isotropic) structure when its crystal size decreases.²

For $n = 1-5$, the lowest-lying energy geometries of Gd_2O_3 clusters are the same as those of Y_2O_3 clusters,²⁴ but the lower-lying geometries are very different. The lowest-lying energy configuration of Gd_2O_3 is a three-dimensional (3D) symmetric bipyramid with D_{3h} group symmetry, which is consistent with previous calculations.^{10,39} Four more isomers with planar structures (1b–1e) lie much higher energetically. The optimal $(\text{Gd}_2\text{O}_3)_2$ cluster is in T_d symmetry. The structure is also the global minimum of those Al_2O_3 ,^{14,20,21} Fe_2O_3 ,²² In_2O_3 ²³ and


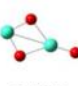
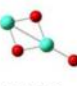
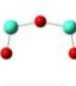
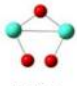


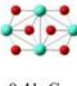
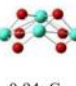
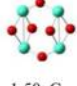

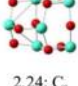
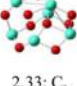


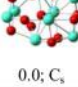
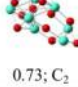
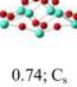
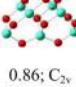
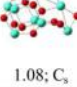
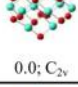
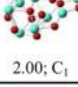
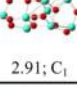
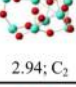
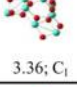
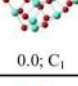
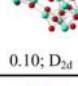
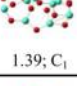
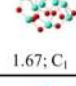
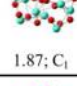
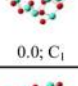
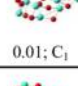
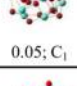
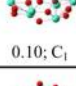
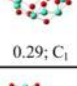
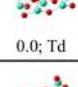
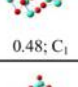
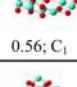
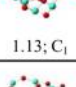

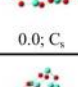
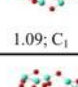
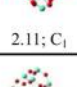
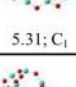
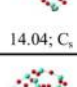
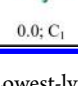
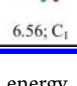

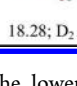
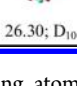
$(\text{Gd}_2\text{O}_3)_n$	(a)	(b)	(c)	(d)	(e)
$n=1$	 2.05; C_s	 2.05; C_s	 2.62; C_{2v}	 3.11; C_s	 5.50; C_{2v}
$n=2$	 0.0; T_d	 0.36; C_s	 0.41; C_{2h}	 0.94; C_{2v}	 1.50; C_{2h}
$n=3$	 0.0; C_{4h}	 2.24; C_s	 2.33; C_s	 2.57; C_s	 3.01; C_1
$n=4$	 0.0; C_s	 0.73; C_2	 0.74; C_s	 0.86; C_{2v}	 1.08; C_s
$n=5$	 0.0; C_{2v}	 2.00; C_1	 2.91; C_1	 2.94; C_2	 3.36; C_1
$n=6$	 0.0; C_1	 0.10; D_{2d}	 1.39; C_1	 1.67; C_1	 1.87; C_1
$n=7$	 0.0; C_1	 0.01; C_1	 0.05; C_1	 0.10; C_1	 0.29; C_1
$n=8$	 0.0; T_d	 0.48; C_1	 0.56; C_1	 1.13; C_1	 1.77; C_s
$n=9$	 0.0; C_s	 1.09; C_1	 2.11; C_1	 5.31; C_1	 14.04; C_s
$n=10$	 0.0; C_1	 6.56; C_1	 17.89; C_1	 18.28; D_2	 26.30; D_{10}

Figure 1. Lowest-lying energy and some of the lower-lying atomic structures of $(\text{Gd}_2\text{O}_3)_n$ ($n = 1-10$) clusters with different symmetries. The energy of an isomer is given with respect to the energy of the lowest-lying isomer for a given size. Spheres in aquamarine and red represent Gd and O atoms, respectively.

Y_2O_3 ²⁴ clusters. In the ground state of $(\text{Gd}_2\text{O}_3)_3$ cluster (3a), six 5-fold coordinated Gd atoms form a symmetric octahedron. One 6-fold coordinated O atom dominates the center and eight 3-fold O atoms cap the eight faces of the octahedron. Four other configurations (3b–3e) without a center oxygen are energetically well above the compact configuration (3a), (2.24, 2.33, 2.57, and 3.01 eV, respectively). The most stable structures for $(\text{Gd}_2\text{O}_3)_4$ and $(\text{Gd}_2\text{O}_3)_5$ are derived from the octahedron configuration of the $(\text{Gd}_2\text{O}_3)_3$ cluster. The data suggests that the compact isomers are more stable than cage-like isomers.

For $n = 6$, the dumbbell-like configuration (6b), which is derived from the octahedron structure of $(\text{Gd}_2\text{O}_3)_3$, presents strong competition with the most stable configuration (6a).

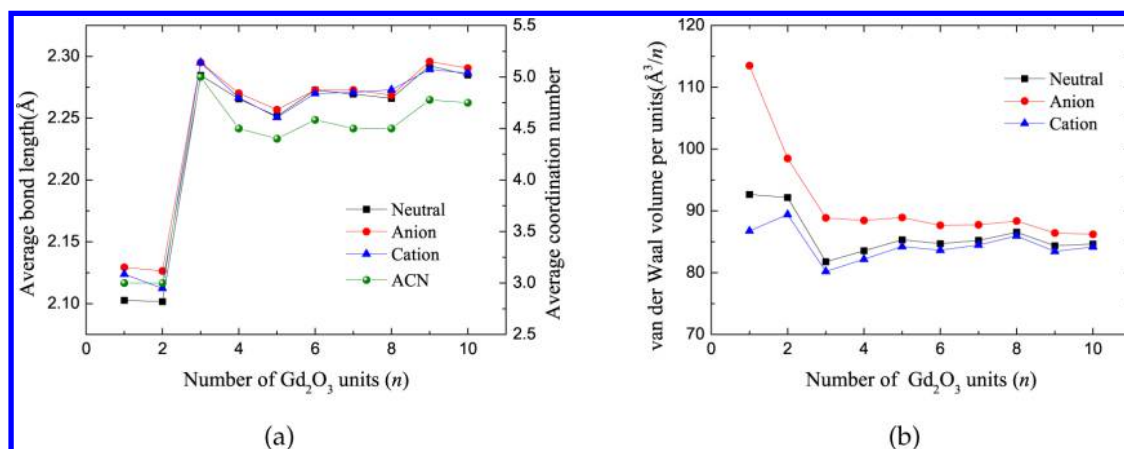


Figure 2. (a) Average coordination number and average bond length for the lowest-energy isomers of $(\text{Gd}_2\text{O}_3)_n^{0,\pm 1}$ clusters with $n = 1-10$; (b) van der Waals volume per unit for the lowest-energy isomers of $(\text{Gd}_2\text{O}_3)_n^{0,\pm 1}$ clusters with $n = 1-10$.

The relative energies of the three low-lying $(\text{Gd}_2\text{O}_3)_7$ structures (7a–7c) are nearly degenerate (0.00, 0.01, and 0.05 eV, respectively). Unlike the $(\text{Y}_2\text{O}_3)_n$ ($n = 6-10$) clusters, whose structures mostly evolve around the octahedron structure of $(\text{Y}_2\text{O}_3)_3$, dense low-symmetry structures are predicted for the global minimums of $(\text{Gd}_2\text{O}_3)_n$ ($n = 6-10$) clusters, as shown in Figure 1. We speculate that stoichiometric $(\text{Gd}_2\text{O}_3)_n$ clusters tend to form globular low-symmetry structures with the successive addition of Gd_2O_3 units. For example, the relative energy of a perfect bubblelike $(\text{Gd}_2\text{O}_3)_{10}$ isomer (10e) with D_{10} symmetry is 26.30 eV, which is much higher than that of the asymmetric isomer (10a). It is also observed that six 4-fold O atoms cap the center Gd in the optimal $(\text{Gd}_2\text{O}_3)_{10}$ cluster (10a). Note that the Gd atoms are 6-fold coordinated and the O atoms are 4-fold coordinated in bulk material.

B. Coordination Number, Bond Length, and van der Waals Volume. To quantitatively describe the geometrical structures of $(\text{Gd}_2\text{O}_3)_n$ ($n = 1-10$) clusters, the average coordination number (ACN) and average bond length (ABL) as functions of the number of Gd_2O_3 units (n) are shown in Figure 2a. The definitions of ACN and ABL are given in section 2 of Supporting Information. The van der Waals volume (V_w)^{40,41} per Gd_2O_3 unit, with a density isosurface value set to 0.002, versus the cluster size n is shown in Figure 2b.

The ABL curves in Figure 2a indicate that the charged particles suffer great deformation for $n = 1$ and 2, but for larger molecular masses ($n \geq 3$), the ABL differences between the ionic and neutral clusters are negligible. The ACN of a cluster remains constant with the addition or removal of an electron. There is a clear preference for a larger ACN for a large structure when $n \geq 3$. Adding (removing) an electron leads to an increase (decrease) in V_w . The charged effect on V_w becomes smaller as the cluster size increases. When $n \geq 3$, the ACN, ABL, and V_w fluctuate slightly with increasing n . Interestingly, the ABL increases but V_w decreases with increasing ACN. The changes in ACN, ABL, and V_w suggest that dense low-symmetry isomers are energetically preferable.

The large ratio of surface atoms in small-sized clusters inherently reduces the ACN value, whereas the favorable compact low-symmetry structure enables an increasing ACN value for a large cluster. The Coulomb repulsion increases with the ACN, which induces the growth trend of the ABL. With the sequential addition of Gd_2O_3 units, the capability of bounding electrons increases for the nucleus, which explains the

decreasing trend of V_w . The removal or addition of an electron affects the electronic density of the population, which causes changes in the interatomic distance and volume of the neutral, anionic, or cationic Gd_2O_3 clusters. The relationship between the ACN, ABL, and V_w as functions of the cluster size makes sense because the distortion directly contributes to many important physical properties.³⁸

C. Binding Energies and Relative Stabilities. The stability of neutral and charged clusters can be characterized by the binding energy (BE) per atom and the fragmentation energy (FE). The BE and FE are calculated as

$$\text{BE: } E_b[(\text{Gd}_2\text{O}_3)_n] = (-E[(\text{Gd}_2\text{O}_3)_n] + 2nE[\text{Gd}] + 3nE[\text{O}]) / (5n) \quad (1)$$

$$\text{FE: } \Delta E[(\text{Gd}_2\text{O}_3)_n] = -E[(\text{Gd}_2\text{O}_3)_n] + E[(\text{Gd}_2\text{O}_3)_{(n-1)}] + E[(\text{Gd}_2\text{O}_3)] \quad (2)$$

where E is the total energy of a cluster. The BE for neutral and ionic $(\text{Gd}_2\text{O}_3)_n$ clusters is shown in Figure 3. The FE for neutral $(\text{Gd}_2\text{O}_3)_n$ clusters is shown in the inset. The BE of cation, neutral, and anion increases with the sequential addition of Gd_2O_3 units. Unlike Ga_2O_3 ¹³ and Y_2O_3 ,²⁴ the addition of an electron causes the $(\text{Gd}_2\text{O}_3)_n$ cluster to become unstable when $n < 4$. When $n \geq 4$, the energy difference is trivial for neutral

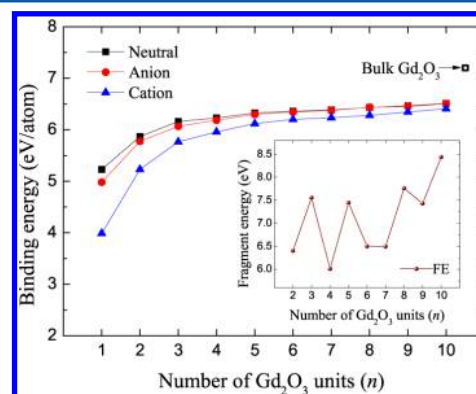


Figure 3. BE and FE (inset chart) for the lowest-energy isomers of $(\text{Gd}_2\text{O}_3)_n$ with $n = 1-10$. The experimental value of bulk cohesive energy (electron volts per atom) for Gd_2O_3 is indicated by a black square with an arrow.

Table 1. AIP, VIP, AEA, VEA, Δ IP, Δ EA, and Fundamental Gap for $(\text{Gd}_2\text{O}_3)_n$ Clusters with $n = 1-10^a$

n	1	2	3	4	5	6	7	8	9	10
AIP	6.20	6.38	5.90	5.40	5.18	4.75	5.26	6.17	5.43	5.05
VIP	6.54	6.75	6.30	5.99	5.80	5.67	5.84	6.51	5.72	5.52
AEA	-1.24	-0.94	-1.42	-0.87	-0.70	-0.46	-0.33	0.09	-0.63	-0.21
VEA	-1.28	-1.25	-1.44	-1.02	-0.78	-0.71	-0.52	-0.24	-0.76	-0.46
AE_g	7.44	7.32	7.32	6.27	5.88	5.21	5.59	6.09	6.06	5.26
VE_g	7.82	8.00	7.73	7.01	6.58	6.38	6.36	6.76	6.49	5.97
Δ IP	-0.34	-0.37	-0.40	-0.59	-0.62	-0.92	-0.58	-0.34	-0.29	-0.47
Δ EA	0.04	0.31	0.02	0.15	0.08	0.25	0.19	0.33	0.13	0.25

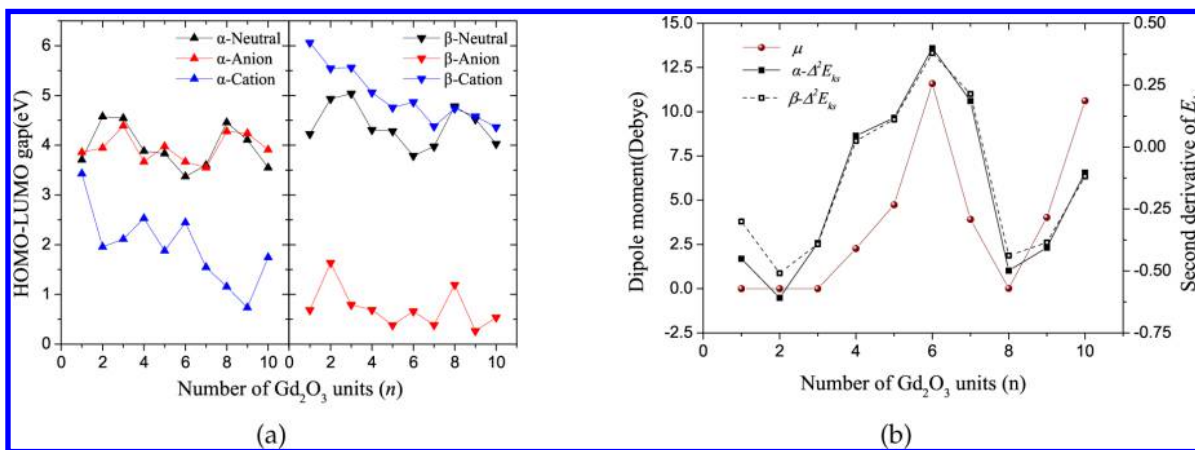
^aAll values are in electronvolts.

Figure 4. (a) HOMO–LUMO gap for the lowest-lying energy isomers of $(\text{Gd}_2\text{O}_3)_n$ clusters with $n = 1-10$. The left- and right-hand graphs show α - E_{KS} and β - E_{KS} , respectively. (b) Dipole moment (μ) and second derivative of the HOMO–LUMO gap ($\Delta^2 E_{KS}$) for the lowest-lying energy isomers of $(\text{Gd}_2\text{O}_3)_n$ clusters with $n = 1-10$.

and anionic isomers. For $n = 10$, the BE per Gd_2O_3 unit is 32.56 eV, which is a little lower than the experimental bulk value (36 eV).⁴² Given the effect of the temperature factor in the experimental measurement, the method in this study is acceptable for the energy calculations of ground states. The FE for $(\text{Gd}_2\text{O}_3)_n$, $n = 2-10$, with respect to the loss of a Gd_2O_3 unit, seems to have oscillatory behavior corresponding to an odd or even n value. Remarkably, the $(\text{Gd}_2\text{O}_3)_{10}$ cluster has the largest fragment energy value (8.43 eV).

D. Electronic Characterization. We list the calculated adiabatic ionization potential (AIP), vertical ionization potential (VIP), adiabatic electron affinity (AEA), and vertical electron affinity (VEA) below. The difference between VIP and AIP (Δ IP) and the difference between VEA and AEA (Δ EA) are given in Table 1. These parameters are of considerable significance in chemisorption. The adiabatic and vertical values of the fundamental gap are also listed in Table 1.

The AIP, VIP, AEA, and VEA^{43,44} are defined as

$$\text{VEA} = E(\text{optimized neut.}) - E(\text{anion at optimized neut. geometry}) \quad (3)$$

$$\text{AEA} = E(\text{optimized neut.}) - E(\text{optimized anion}) \quad (4)$$

$$\text{VIP} = E(\text{cation at optimized neut. geometry}) - E(\text{optimized neut.}) \quad (5)$$

$$\text{AIP} = E(\text{optimized cation}) - E(\text{optimized neut.}) \quad (6)$$

The theoretical definition of the fundamental gap (E_g) is the difference between the molecular ionization potential (IP) and

electron affinity (EA).^{45,46} The IP and EA values for the lowest-lying isomers do not show any regular changes when n grows from 1 to 10. The difference between VIP and AIP is greater than that between VEA and AEA, indicating that the cation is subject to more topological distortion than the anion in the ground state. This is also in agreement with our previous analysis of BE in section 3C.

According to Table 1, the vertical E_g (VE_g) is generally slightly larger than the adiabatic E_g (AE_g) at a fixed n . For $n = 10$, the vertical E_g is 5.97 eV and the adiabatic E_g is 5.26 eV. The variations between the vertical and adiabatic E_g are due to the topological differences in the ground-state configurations. Note that the experimental band gap for bulk c- Gd_2O_3 is 5.9 ± 0.1 eV and for a- Gd_2O_3 is 5.8 ± 0.1 eV.^{47–49} Compared with the HOMO–LUMO gap in Figure 4a, the fundamental gap can serve as a better predictor of the energy gap.

The KS gap (E_{KS}) is defined as the energy difference between the lowest unoccupied molecular orbital and the highest occupied molecular orbital, also called the HOMO–LUMO gap.^{45,46} Both α and β HOMO–LUMO gaps are plotted in Figure 4a. As pointed out in previous reports,^{45,46} there is a band gap problem with density functional theory. The α and β HOMO–LUMO gaps are much smaller than the vertical and adiabatic E_g for neutral $(\text{Gd}_2\text{O}_3)_n$ clusters, as $E_g = E_{KS} + \Delta_{xc}$, where Δ_{xc} represents the derivative discontinuity of exchange–correlation energy.⁴⁵ However, E_{KS} is proved to be accordant with the first excitation energy (the optical gap).^{50–54} Interestingly, the behavior of the HOMO–LUMO gaps correlate very well with the vertical fundamental gap for neutral nanoparticles.

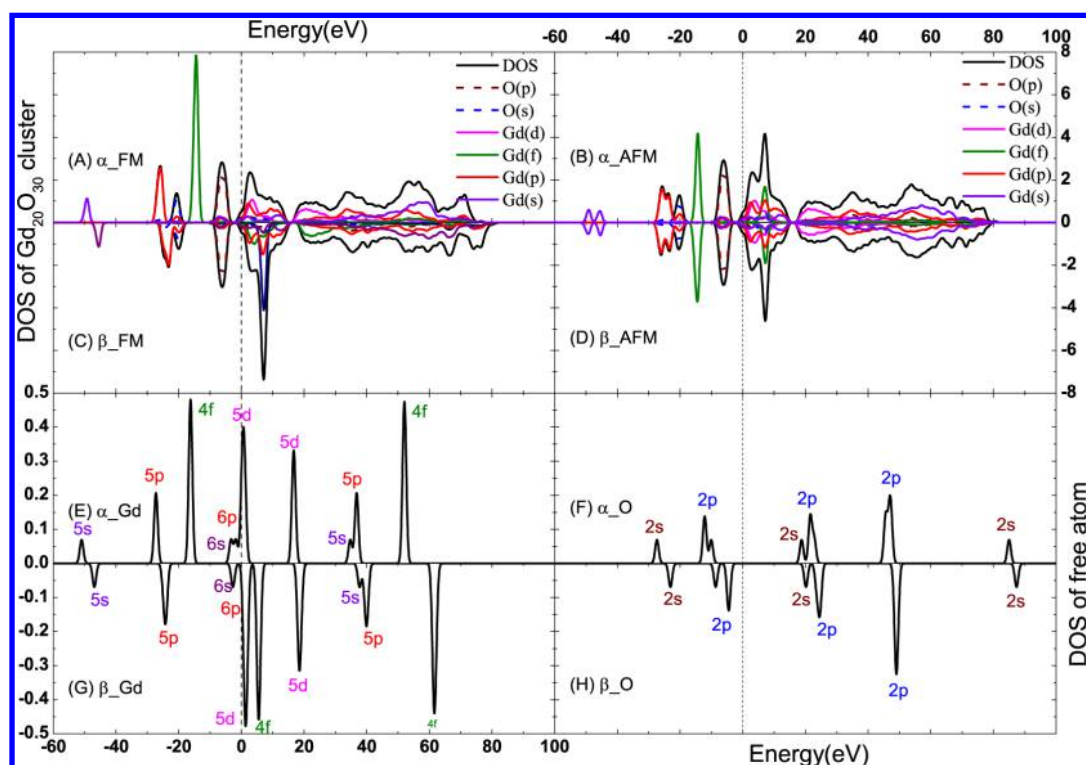


Figure 5. (A–H) Total and orbital-projected partial DOS for the $(\text{Gd}_2\text{O}_3)_{10}$ cluster, along with the DOS of free Gd and O atoms.

Table 2. HOMO–LUMO (E_{KS}) Energy Gap of $(\text{Gd}_2\text{O}_3)_n$ ($n = 1–10$) Clusters in the FM and AFM States

	1	2	3	4	5	6	7	8	9	10
α - E_{KS} in FM state	3.71	4.58	4.54	3.88	3.83	3.64	3.60	4.46	4.11	3.55
β - E_{KS} in FM state	4.23	4.93	5.04	4.31	4.28	3.79	3.97	4.78	4.52	3.97
α - E_{KS} in AFM state	3.86	4.62	4.69	3.99	3.99	3.71	3.91	4.58	4.26	3.90
β - E_{KS} in AFM state	3.86	4.62	4.69	4.11	3.99	3.44	3.65	4.59	4.18	3.65

Clearly, there is an opposite trend for α and β HOMO–LUMO gaps of ionic clusters. For the α molecular orbital (spin-up channel), a neutral cluster possesses almost the same E_{KS} value as that of an anionic cluster and a much higher value than that of a cationic cluster. In contrast, for the β molecular orbital (spin-down channel), the E_{KS} value of the anionic isomer is much lower than those of the neutral and cationic isomers, suggesting that the removed electron comes from the α -HOMO orbital and the extra electron fills the β -LUMO orbital. This assumption finds evidence in the frontier orbital analysis, in the image of HOMO and LUMO for neutral and ionic Gd_6O_9 clusters (shown in section 3 of Supporting Information).

In Figure 4b, we present the second derivative of the α and β HOMO–LUMO gaps ($\Delta^2 E_{\text{KS}}$) and the dipole moment (μ) against the number of Gd_2O_3 units (n) for the lowest-lying energy structures. From the increasing BE and the fluctuations in E_{g} , E_{KS} , and μ , we can infer that E_{g} , E_{KS} , and μ have no strong relevance to the stability of the clusters. The stabilities of large structures are attributable to the effect of the atom arrangement rather than electronic closure. The dipole moment correlates very well with the second derivative of the α and β HOMO–LUMO gaps. To some extent, $\Delta^2 E_{\text{KS}}$ presents the intensity of the electrical potential, which is mainly determined by the geometrical structure, and μ corresponds to the asymmetrical charge distribution and always aligns itself with the electric field; thus, it is sensitively dependent on $\Delta^2 E_{\text{KS}}$.

E. Magnetic Properties. We made AFM coupling guesses based on the optimized neutral geometries in the highest spin states (FM states). After optimization, the structures are almost unchanged. One can infer that the Gd-4f orbitals participate weakly in bonding; therefore, the 4f patterns weakly affect their structures. A representative, natural population analysis was performed for the AFM and FM states of the lowest-lying energy $(\text{Gd}_2\text{O}_3)_{10}$ cluster (shown in section 4 of Supporting Information). The occupation value (around seven electrons) of the Gd-4f orbital is nearly the same as that with the free Gd^{3+} , which indicates that the Gd-4f orbital rarely participates in bonding. To have a clear view of the bonding characters and electronic structures of $(\text{Gd}_2\text{O}_3)_n$ clusters, we present the total density of states (DOS) and the orbital-projected partial DOS for the ground state of $(\text{Gd}_2\text{O}_3)_{10}$ clusters (Figure 5). We used the modified Mulliken population defined by Ros and Schuit (the SCPA method) to implement the calculations.⁵⁵

The analysis of DOS/PDOS indicates that the HOMO level is mainly dominated by the O-2p orbital and the LUMO level is dominated primarily by the Gd-6s orbital and partially by the Gd-6p orbital. We present the electron density isosurfaces for the HOMO and LUMO states of the lowest-lying energy $(\text{Gd}_2\text{O}_3)_{10}$ cluster in Figure 3 of Supporting Information. With respect to the energy level of isolated Gd and O atoms, the ground state of the $(\text{Gd}_2\text{O}_3)_{10}$ cluster has an overall downshift of Gd-6s, Gd-6p orbitals and an upshift (downshift) of spin-up (spin-down) O-2p orbitals, leading to a slight overlap of these

orbitals. We observe a slightly larger overlap between the Gd-5p and O-2 s orbitals. Above the LUMO level, there is a high degree of hybridization, which may explain the low stabilities of the ultrasmall Gd₂O₃ cluster. The Gd-4f orbitals are strongly localized in both the FM and AFM states. In the AFM state, the Gd-4f band splits into two sub-bands, whereas in the FM state, the spin-up and spin-down Gd-4f orbitals are well separated by 21.66 eV.

The HOMO–LUMO gaps (E_{KS}) are listed in Table 2. In the FM states, the β - E_{KS} values are higher than the α - E_{KS} values. In the AFM states, however, the β - E_{KS} values are nearly identical to the α - E_{KS} values for the symmetry structures (e.g., $n = 1$ –5, 8), but are lower than the α - E_{KS} values for the asymmetry structures (e.g., $n = 6, 7, 9, 10$). E_{KS} shows a correlation with point group symmetry rather than cluster size. Overall, both α - E_{KS} and β - E_{KS} in the AFM states are between those in the FM states.

The total energy difference (ΔE) and BE difference (ΔBE) between the AFM and FM states for the global minima are shown in Figure 6. Because J signifies the spin–spin interaction

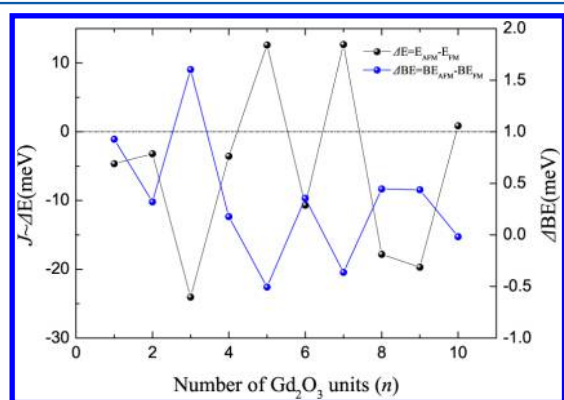


Figure 6. Dependence of exchange coupling $J \sim \Delta E$ and ΔBE on the number of Gd₂O₃ units for the lowest-lying energy clusters.

that can be extracted by mapping the energies of spin states onto the Hamiltonian, ΔE was used to evaluate the magnetic exchange parameter J .⁵⁶ It is clear that the energy differences (J) between the AFM and FM states are quite small, ranging from -24.04 to 12.62 meV. The small magnitude of J suggests that the ground state is easily alternated to the excited state. At room temperature, the nanoparticles demonstrate paramagnetic properties because the spin reversal barrier is easily compensated by thermal population.

Obviously, there is a contrast between the trends of ΔE and ΔBE . Both show oscillatory behavior with the successive addition of Gd₂O₃ units. For $n = 1$ –4 and 6, the ground states of the clusters are in AFM states, which agrees with the results of previous studies.^{10,18,39} However, for (Gd₂O₃)₅ and (Gd₂O₃)₇, whose magnetism has been neglected by other researchers, the FM states are energetically more preferable than the AFM states. For $n = 10$, the corresponding FM state has almost the identical energy as the AFM state ($\Delta E = 0.87$ meV). The Gd³⁺O²⁻–Gd³⁺ superexchange can interpret the AFM in the Gd₂O₃ bulk, and the Ruderman–Kittel–Kasuya–Yosida (RKKY) interaction can illustrate the FM in the Gd bulk, which may shed light on the magnetic oscillation behavior of (Gd₂O₃)_n clusters.^{27–29,56–58} Recently, Chen and co-workers performed uniform compression and expansion of the lowest-lying energy Gd₈O₁₂ cluster and found that the strengths of the

FM RKKY interaction and AFM superexchange interaction were comparable in the range of medium Gd–O distances (2.0–2.6 Å).¹⁰ Unlike their report, the Gd-4f orbitals in this study are strongly localized, so the superexchange type of Gd-4f orbitals with O-2p orbitals is effectively precluded, which is consistent with most of the studies on the gadolinium element and its compounds.^{17,18,28–30,57,59,60}

However, the potential from the 4f⁷ core affects the character of valence 5d and 6s electrons for the Gd atom, which presents a substantial interatomic exchange interaction. Similar to the results reported in ref 61, the Gd-6p orbital plays an important role in the magnetic interaction of the (Gd₂O₃)_n cluster. To verify our hypothesis, we calculated the J values for various (Gd₂O₃)₆ clusters (shown in section 5 of Supporting Information). Magnetic oscillation is also observed for $n = 6$. The results may clarify both the long debate on the issue and the superparamagnetic properties of large Gd₂O₃ nanoparticles.⁶⁰ Thus, we may conclude that the magnetic fluctuation of (Gd₂O₃)_n clusters can be illustrated by the competition between RKKY-type and superexchange-type interactions.

IV. CONCLUSION

We calculated the structural, electronic, and magnetic properties of (Gd₂O₃)_n^{0,±1} clusters with $n = 1$ –10 using SDFT calculations within the broken-symmetry approach and quantitatively studied extensive cluster structures in the FM and AFM states.

Size-induced changes in the point symmetry were observed in the (Gd₂O₃)_n clusters. The symmetry of the (Gd₂O₃)_n^{0,±1} cluster reduces as cluster size increases, and the BE of the cluster also increases with cluster size. The average bonding length increases with the coordinate number. The dipole moment correlates well with the second derivative of the HOMO–LUMO gap. Compared with the experimental measurements, the fundamental gap is better for predicting the energy gap for Gd₂O₃ nanoparticles.

There is a magnetic oscillation in the lowest-lying energy (Gd₂O₃)_n clusters with $n = 1$ –10. The various structures of Gd₁₂O₁₈ also show similar behavior. This oscillation can be interpreted as competition between the AFM superexchange-type and FM RKKY-type interactions. The magnetic property of the cluster is predominately decided by the arrangement of atoms and bonding length. The energy difference between the AFM and FM states at fixed n is quite small, indicating that the AFM state is easily alternated to the FM state.

As (Gd₂O₃)_n nanoparticles can serve as potential multimodal imaging and therapeutic agents, we hope that the current calculations on stoichiometric clusters of different sizes will provide an impetus for further experimental and theoretical studies on Gd₂O₃.

■ ASSOCIATED CONTENT

● Supporting Information

Details of benchmark calculations, definitions of ACN and ABL, electron density isosurfaces for Gd₆O₉, natural population analysis of (Gd₂O₃)₁₀, and magnetic properties of (Gd₂O₃)₆. This material is available free of charge via the Internet at <http://pubs.acs.org>.

■ AUTHOR INFORMATION

Corresponding Author

*E-mail: stssyz@mail.sysu.edu.cn.

Notes

The authors declare no competing financial interest.

ACKNOWLEDGMENTS

This study was supported by the Natural Science Foundation of China (Grant 11274394), the Natural Science Foundation of Guangdong Province (Grant S2012010010542), the Fundamental Research Funds for the Central Universities (Grant 11lgjc12), and the Specialized Research Fund for the Doctoral Program of Higher Education (Grant 20110171110023).

REFERENCES

- Segura, M.; Kadankov, M.; Mateos, X.; Pujol, M.; Carvajal, J.; Aguiló, M.; Díaz, F.; Griebner, U.; Petrov, V. Polarization Switching in the $2\mu\text{m}$ Tm:KLu(WO₄)₂ Laser. *Laser Phys. Lett.* **2012**, *9*, 104–109.
- Wang, F.; Han, Y.; Lim, C. S.; Lu, Y.; Wang, J.; Xu, J.; Chen, H.; Zhang, C.; Hong, M.; Liu, X. Simultaneous Phase and Size Control of Upconversion Nanocrystals through Lanthanide Doping. *Nature* **2010**, *463*, 1061–1065.
- Paik, T.; Gordon, T. R.; Prantner, A. M.; Yun, H.; Murray, C. B. Designing Tripodal and Triangular Gadolinium Oxide Nanoplates and Self-Assembled Nanofibrils as Potential Multimodal Bioimaging Probes. *ACS Nano* **2013**, *7*, 2850–2859.
- Chen, L.; Han, S.; Wang, Z.; Wang, J.; Zhang, H.; Yu, H.; Han, S.; Xu, X. Controlling Laser Emission by Selecting Crystal Orientation. *Appl. Phys. Lett.* **2013**, *102*, 011137.
- Lehmusvuori, A.; Manninen, J.; Huovinen, T.; Soukka, T.; Lamminmäki, U. Homogenous M₁₃ Bacteriophage Quantification Assay Using Switchable Lanthanide Fluorescence Probes. *BioTechniques* **2012**, *53*, 301–303.
- Kim, T.; Chae, K.; Chang, Y.; Lee, H. Gadolinium Oxide Nanoparticles as Potential Multimodal Imaging and Therapeutic Agents. *Curr. Top. Med. Chem. (Sharjah, United Arab Emirates)* **2013**, *13*, 422–433.
- Yang, G.; Lv, R.; Gai, S.; Dai, Y.; He, F.; Yang, P. Multifunctional SiO₂@Gd₂O₃:Yb/Tm Hollow Capsules: Controllable Synthesis and Drug Release Properties. *Inorg. Chem.* **2014**, *53*, 10917–10927.
- Fang, J.; Chandrasekharan, P.; Liu, X. L.; Yang, Y.; Lv, Y. B.; Yang, C. T.; Ding, J. Manipulating the Surface Coating of Ultra-Small Gd₂O₃ Nanoparticles for Improved T1-weighted MR Imaging. *Biomaterials* **2014**, *35*, 1636–1642.
- Shao, Y. Z.; Tian, X. M.; Hu, W. Y.; Zhang, Y. Y.; Liu, H.; He, H. Q.; Shen, Y. Y.; Xie, F. K.; Li, L. The Properties of Gd₂O₃-Assembled Silica Nanocomposite Targeted Nanoprobes and Their Application in MRI. *Biomaterials* **2012**, *33*, 6438–6446.
- Yuan, H. K.; Chen, H.; Tian, C. L.; Kuang, A. L.; Wang, J. Z. Density Functional Calculations for Structural, Electronic, and Magnetic Properties of Gadolinium-oxide Clusters. *J. Chem. Phys.* **2014**, *140*, 154308.
- Jia, G.; Liu, K.; Zheng, Y.; Song, Y.; Yang, M.; You, H. Highly Uniform Gd(OH)₃ and Gd₂O₃:Eu³⁺ Nanotubes: Facile Synthesis and Luminescence Properties. *J. Phys. Chem. C* **2009**, *113*, 6050–6055.
- Cao, Y. C. Synthesis of Square Gadolinium-oxide Nanoplates. *J. Am. Chem. Soc.* **2004**, *126*, 7456–7457.
- Yang, J.; Li, C.; Cheng, Z.; Zhang, X.; Quan, Z.; Zhang, C.; Lin, J. Size-Tailored Synthesis and Luminescent Properties of One-Dimensional Gd₂O₃:Eu³⁺ Nanorods and Microrods. *J. Phys. Chem. C* **2007**, *111*, 18148–18154.
- Li, W.; Zheng, X.; Li, F.; Wang, J. Facile Synthetic Route to Hollow Gadolinium Oxide Spheres with Tunable Thickness. *Nano Lett.* **2012**, *7*, 1267–1269.
- Gai, S.; Li, C.; Yang, P.; Lin, J. Recent Progress in Rare Earth Micro/Nanocrystals: Soft Chemical Synthesis, Luminescent Properties, and Biomedical Applications. *Chem. Rev. (Washington, DC, U.S.)* **2014**, *114*, 2343–2389.
- Xu, L.; Dong, B.; Wang, Y.; Bai, X.; Chen, J.; Liu, Q.; Song, H. Porous In₂O₃:RE (RE = Gd, Tb, Dy, Ho, Er, Tm, Yb) Nanotubes: Electrospinning Preparation and Room Gas-sensing Properties. *J. Phys. Chem. C* **2010**, *114*, 9089–9095.
- Pedersen, H.; Ojamäe, L. Towards Biocompatibility of RE₂O₃ Nanocrystals - Water and Organic Molecules Chemisorbed on Gd₂O₃ and Y₂O₃ Nanocrystals Studied by Quantum-chemical Computations. *Nano. Lett.* **2006**, *6*, 2004–2008.
- Ning, L.; Zhang, Y.; Cui, Z.; Trioni, M. L.; Brivio, G. P. Density Functional Theory Study of Magnetic Coupling in the Gd₁₂O₁₈ Cluster. *J. Phys. Chem. A* **2008**, *112*, 13650–13654.
- Frisch, M. J.; Trucks, G. W.; Schlegel, H. B.; Scuseria, G. E.; Robb, M. A.; Cheeseman, J. R.; Scalmani, G.; Barone, V.; Mennucci, B.; Petersson, G. A.; et al. *Gaussian09*, revision d.01; Gaussian Inc.: Wallingford, CT, 2009.
- Sun, J.; Lu, W. C.; Zhang, W.; Zhao, L. Z.; Li, Z. S.; Sun, C. C. Theoretical Study on (Al₂O₃)_n (n = 1–10 and 30) Fullerenes and H₂ Adsorption Properties. *Inorg. Chem.* **2008**, *47*, 2274–2279.
- Rahane, A. B.; Deshpande, M. D.; Kumar, V. Structural and Electronic Properties of (Al₂O₃)_n Clusters with n = 1–10 from First Principles Calculations. *J. Phys. Chem. C* **2011**, *115*, 18111–18121.
- Ding, X. L.; Xue, W.; Ma, Y. P.; Wang, Z. C.; He, S. G. Density Functional Study on Cage and Noncage (Fe₂O₃)_n Clusters. *J. Chem. Phys.* **2009**, *130*, 014303.
- Görbitz, C. H.; Dalhus, B.; Day, G. M. Pseudoracemic Amino Acid Complexes: Blind Predictions for Flexible Two-Component Crystals. *Phys. Chem. Chem. Phys.* **2010**, *12*, 8466–77.
- Rahane, A. B.; Murkute, P.; Deshpande, M. D.; Kumar, V. Density Functional Calculations of the Structural and Electronic Properties of (Y₂O₃)_n^{0,±1} (Clusters with n = 1–10). *J. Phys. Chem. A* **2013**, *117*, 5542–5550.
- Ding, X. L.; Li, Z. Y.; Meng, J. H.; Zhao, Y. X.; He, S. G. Density-Functional Global Optimization of (La₂O₃)_n Clusters. *J. Chem. Phys.* **2012**, *137*, 214311.
- Li, L.; Cheng, L. First Principle Structural Determination of (B₂O₃)_n (n = 1–6) Clusters: From Planar to Cage. *J. Chem. Phys.* **2013**, *138*, 094312.
- Dai, D.; Whangbo, M. H. Spin Exchange Interactions of a Spin Dimer: Analysis of Broken-Symmetry Spin States in Terms of the Eigenstates of Heisenberg and Ising Spin Hamiltonians. *J. Chem. Phys.* **2003**, *118*, 29–39.
- Roy, L. E.; Hughbanks, T. Magnetic Coupling in Dinuclear Gd Complexes. *J. Am. Chem. Soc.* **2006**, *128*, 568–575.
- Roy, L.; Hughbanks, T. d-Electron Mediated 4fⁿ–4fⁿ Exchange in Gd-Rich Compounds; Spin Density Functional Study of Gd₂Cl₃. *J. Solid State Chem.* **2003**, *176*, 294–305.
- Sweet, L. E.; Roy, L. E.; Meng, F.; Hughbanks, T. Ferromagnetic Coupling in Hexanuclear Gadolinium Clusters. *J. Am. Chem. Soc.* **2006**, *128*, 10193–10201.
- Lee, C.; Hill, C.; Carolina, N. Development of the Colle-Salvetti Correlation-Energy Formula into a Functional of the Electron Density. *Phys. Rev. B: Condens. Matter Mater. Phys.* **1988**, *37*, 785–789.
- Stevens, W. J.; Basch, H.; Krauss, M. Compact Effective Potentials and Efficient Shared-Exponent Basis Sets for the First- and Second-row Atoms. *J. Chem. Phys.* **1984**, *81*, 6026.
- Curtiss, L.; Raghavachari, K.; Pople, J. Gaussian-2 Theory Using Reduced Møller–Plesset Orders. *J. Chem. Phys.* **1993**, *98*, 1293.
- Stevens, W.; Krauss, M.; Basch, H.; Paul, G. Relativistic Compact Effective Potentials and Efficient, Shared-Exponent Basis Sets for the Third-, Fourth-, and Fifth-Row Atoms. *Can. J. Chem.* **1991**, *70*, 612–630.
- Rassolov, V.; Ratner, M.; Pople, J.; Redfern, P. C.; Curtiss, L. 6-31G* Basis Set for Third-Row Atoms. *J. Comput. Chem.* **2001**, *22*, 976–984.
- Rassolov, V.; Pople, J.; Ratner, M.; Windus, T. L. 6-31G Basis Set for Atoms K through Zn. *J. Chem. Phys.* **1998**, *109*, 1223–1229.
- Lu, T.; Chen, F. Multiwfn: A Multifunctional Wavefunction Analyzer. *J. Comput. Chem.* **2012**, *33*, 580–592.
- Ayyub, P.; Palkar, V. R.; Chattopadhyay, S.; Multani, M.; Road, B. Effect of Crystal Size Reduction on Lattice Symmetry and

- Cooperative Properties. *Phys. Rev. B: Condens. Matter Mater. Phys.* **1995**, *51*, 6135–6138.
- (39) Ayuela, A.; March, N. H.; Klein, D. J. Optimized Geometry of the Cluster Gd_2O_3 and Proposed Antiferromagnetic Alignment of F-Electron Magnetic Moment. *J. Phys. Chem. A* **2007**, *111*, 10162–10165.
- (40) Kusumaatmaja, H.; Wales, D. J. Defect Motifs for Constant Mean Curvature Surfaces. *Phys. Rev. Lett.* **2013**, *110*, 165502.
- (41) Vydrov, O. A.; Voorhis, T. V. Nonlocal van der Waals Density Functional Made Simple. *Phys. Rev. Lett.* **2009**, *063004*, 7–10.
- (42) Crist, B. V. *Handbook of Monochromatic XPS Spectra*; XPS International: Mountain View, CA, 1999; Vol. 1, pp 85–90.
- (43) Kiracofe, J. C.; Tschumper, G. S.; Schaefer, H. F.; Nandi, S.; Ellison, G. B. Atomic and Molecular Electron Affinities: Photoelectron Experiments and Theoretical Computations. *Chem. Rev. (Washington, DC, U.S.)* **2002**, *102*, 231–282.
- (44) Ga, O.; Clusters, G.; Gowtham, S.; Deshpande, M.; Costales, A.; Pandey, R. Structural, Energetic, Electronic, Bonding, and Vibrational Properties of Ga_3O , Ga_3O_2 . *J. Phys. Chem. B* **2005**, *109*, 14836–14844.
- (45) Stein, T.; Eisenberg, H.; Kronik, L.; Baer, R. Fundamental Gaps in Finite Systems from Eigenvalues of a Generalized Kohn-Sham Method. *Phys. Rev. Lett.* **2010**, *105*, 266802.
- (46) Baerends, E. J.; Gritsenko, O. V.; van Meer, R. The Kohn-Sham Gap, the Fundamental Gap and the Optical Gap: The Physical Meaning of Occupied and Virtual Kohn-Sham Orbital Energies. *Phys. Chem. Chem. Phys.* **2013**, *15*, 16408–16425.
- (47) Robertson, J.; Falabretti, B. Band Offsets of High K Gate Oxides on III-V Semiconductors. *J. Appl. Phys.* **2006**, *100*, 014111.
- (48) Afanas'ev, V. V.; Shamuilia, S.; Stesmans, A.; Dimoulas, A.; Panayiotatos, Y.; Sotiropoulos, A.; Houssa, M.; Brunco, D. P. Electron Energy Band Alignment at Interfaces of (100)Ge with Rare-Earth Oxide Insulators. *Appl. Phys. Lett.* **2006**, *88*, 2004–2007.
- (49) Badylevich, M.; Shamuilia, S.; Afanas, V. V.; Stesmans, A.; Laha, A.; Osten, H. J.; Fissel, A. Investigation of the Electronic Structure at Interfaces of Crystalline and Amorphous Gd_2O_3 Thin Layers with Silicon Substrates of Different Orientations. *Rev. Mod. Phys.* **2009**, *99*, 252101.
- (50) Kümmel, S.; Kronik, L. Orbital-Dependent Density Functionals: Theory and Applications. *Rev. Mod. Phys.* **2008**, *80*, 3–60.
- (51) Salzner, U.; Lagowski, J. B.; Pickup, P. G.; Poirier, R. A. Design of Low Band Gap Polymers Employing Density Functional Theory. *J. Comput. Chem.* **1997**, *18*, 1943–1953.
- (52) Barone, V.; Peralta, J. E.; Wert, M.; Heyd, J.; Scuseria, G. E. Density Functional Theory Study of Optical Transitions in Semiconducting Single-Walled Carbon Nanotubes. *Nano. Lett.* **2005**, *5*, 1621–1624.
- (53) Dori, N.; Menon, M.; Kilian, L.; Sokolowski, M.; Kronik, L.; Umbach, E. Valence Electronic Structure of Gas-Phase 3,4,9,10-Perylene Tetracarboxylic Acid Dianhydride: Experiment and Theory. *Phys. Rev. B: Condens. Matter Mater. Phys.* **2006**, *73*, 1–6.
- (54) Zhan, C. G.; Nichols, J.; Dixon, D. Ionization Potential, Electron Affinity, Electronegativity, Hardness, and Electron Excitation Energy: Molecular Properties from Density Functional Theory Orbital Energies. *J. Phys. Chem. A* **2003**, *107*, 4184–4195.
- (55) Mercier, B.; Ledoux, G.; Dujardin, C.; Nicolas, D.; Masenelli, B.; Mélinon, P.; Bergeret, G. Quantum Confinement Effect on Gd_2O_3 Clusters. *J. Chem. Phys.* **2007**, *126*, 044507.
- (56) Phillips, J. J.; Peralta, J. E. Magnetic Exchange Couplings from Semilocal Functionals Evaluated Nonself-Consistently on Hybrid Densities: Insights on Relative Importance of Exchange, Correlation, and Delocalization. *J. Chem. Theory Comput.* **2012**, *8*, 3147–3158.
- (57) Joon, M.; Ozaki, T.; Yu, J.; Han, M. J. Effect of on-Site Coulomb Interactions on the Electronic Structure and Magnetic Property of Gd_2 Cluster. *Chem. Phys. Lett.* **2010**, *492*, 89–92.
- (58) Yuan, H. K.; Chen, H.; Kuang, A. L.; Wu, B. Geometrical Structure and Spin Order of Gd_{13} Cluster. *J. Chem. Phys.* **2011**, *135*, 114512.
- (59) Gillen, R.; Clark, S.; Robertson, J. Nature of the Electronic Band Gap in Lanthanide Oxides. *Phys. Rev. B: Condens. Matter Mater. Phys.* **2013**, *87*, 125116.
- (60) Jia, G.; You, H.; Liu, K.; Zheng, Y.; Guo, N.; Zhang, H. Highly Uniform Gd_2O_3 Hollow Microspheres: Template-Directed Synthesis and Luminescence Properties. *Langmuir* **2010**, *26*, 5122–5128.
- (61) Gutsev, G. L.; Johnson, L. E.; Belay, K. G.; Weatherford, C.; Gutsev, L. G.; Ramu Ramachandran, B. Structure and Magnetic Properties of Fe_nGd Clusters, $n = 12–19$. *Eur. Phys. J. D* **2014**, *68*, 1–9.